Supplementary Information

3D-printed implantable CAR-macrophages for post-surgery cancer immunotherapy

Dingmeng Nie[1,2,#], Yang Shen[2,3,4,#], Yangtao Xu[2,5,#], Xiao Hu[2,6], Jiayang Qiu[1], Xinyao Hu[2,5], Qian-Fang Meng[2], Peng She[6,*], Lang Rao[2,3,*], and Qinqin Huang[1,*]

[1] School of Electronic and Electrical Engineering, Wuhan Textile University, Wuhan 430200, China.

[2] Institute of Chemical Biology, Shenzhen Bay Laboratory, Shenzhen 518132, China.

[3] Shenzhen Medical Academy of Research and Translation (SMART), Shenzhen 518107, China.

[4] Westlake University, Hangzhou 310030, China.

[5] Cancer Center, Renmin Hospital of Wuhan University, Wuhan 430060, China.

[6] Department of Orthopedics, The Seventh Affiliated Hospital of Sun Yat-Sen University, Shenzhen 518000, China.

[#] These authors contributed equally to this work.

* Corresponding e-mail: shep@mail.sysu.edu.cn (P.S.); lrao@szbl.ac.cn (L.R.); and qqhuang@zzu.edu.cn (Q.H.).

Supplementary Figures

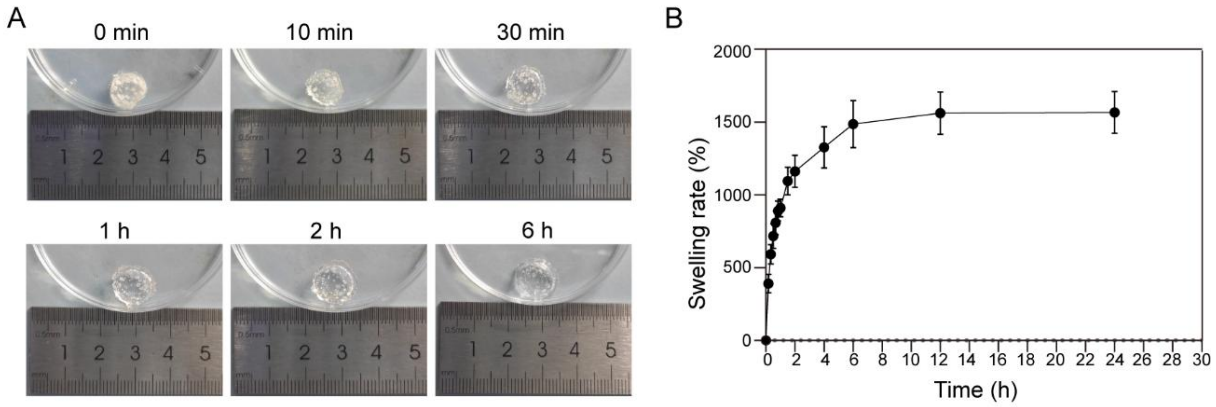

Figure S1. Swelling behavior and equilibrium swelling ratio of the hydrogel. (A) Representative images of the hydrogel at different times during swelling (0 min, 10 min, 30 min, 1 h, 2 h, and 6 h). (B) The swelling kinetic curve shows an increase in swelling ratio over time until equilibrium is reached.

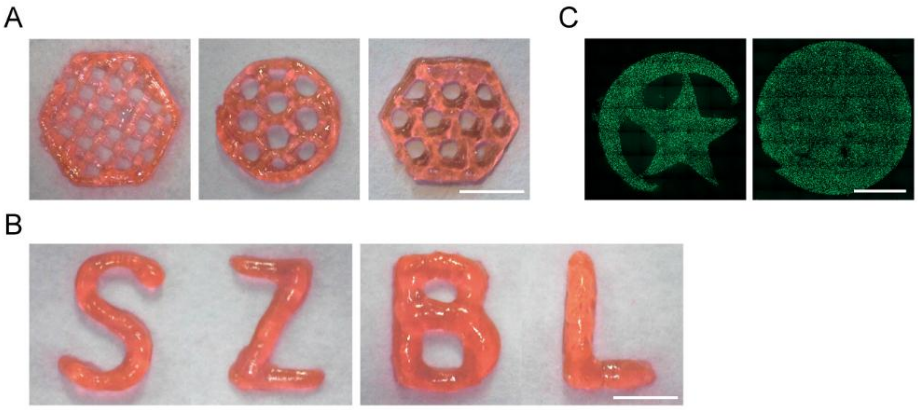

Figure S2. Fabrication and multi-shape printing capacity of the 3D-bioprinted scaffold hydrogel. (A) 3D-printed scaffolds with different designed geometries. Scale bar, 5 mm. (B) Scaffolds printed into various letter shapes demonstrate printing precision and multi-shape capability. Scale bar, 5 mm. (C) 3D bioprinting of cell-laden hydrogel into complex structures. Fluorescence imaging confirms uniform cell distribution within the printed structures. Scale bar, 5 mm.

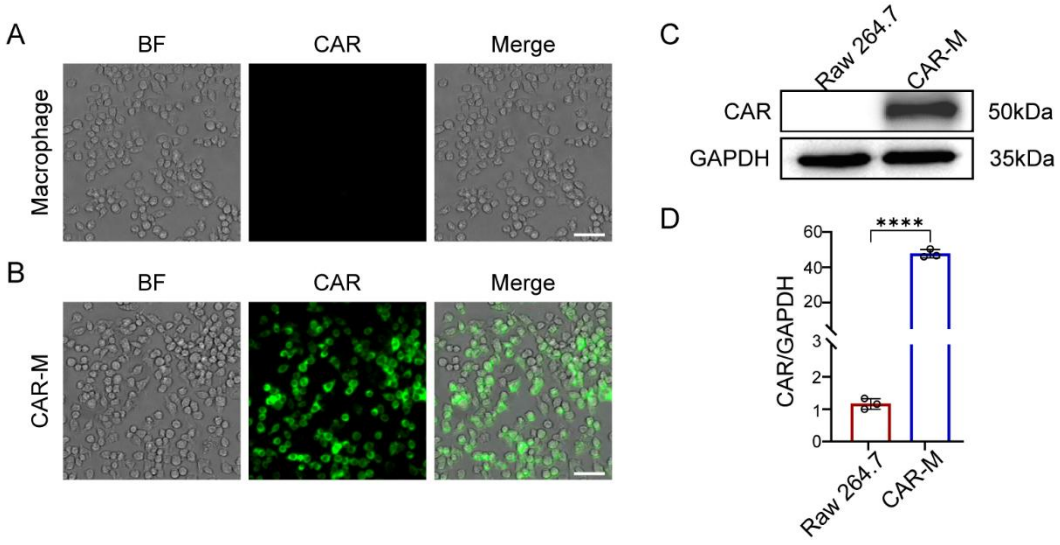

Figure S3. Characterization of CAR-M confirms successful CAR transfection. (A-B) Fluorescence images show bright field (BF), CAR expression (CAR), and merged view (Merge) for both untransfected macrophages and CAR-M. The CAR signal indicates successful expression and membrane localization. Scale bar, 50 μm. (C-D) Western blot and quantitative analysis validating CAR expression in transfected macrophages. Protein lysates from untransfected Raw 264.7 cells and CAR-M were probed with antibodies against CAR and GAPDH (loading control). Data are presented as mean ± s.d. ($n = 3$). Statistical significance was calculated via unpaired two-tailed t-test. ns, no significance. ****$p < 0.0001$.

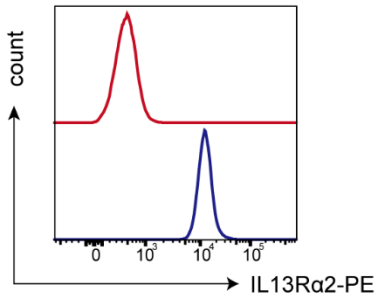

Figure S4. Construction and validation of 4T1-IL13Rα2 stable cell line. Flow cytometry histogram showing IL13Rα2 surface expression on transduced 4T1 cells (related to Figure 3A).

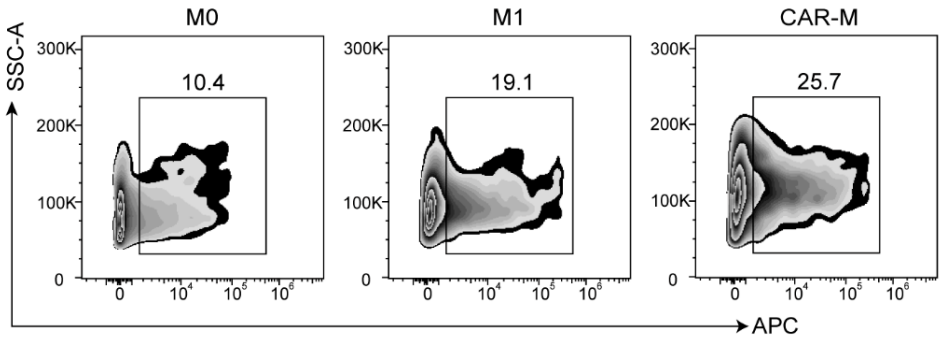

Figure S5. Flow cytometric quantification of target cell phagocytosis by macrophages. Representative flow cytometry plots showing APC$^+$ for M0, M1, and CAR-M populations after co-culturing with APC-labeled 4T1-IL13Rα2 target cells.

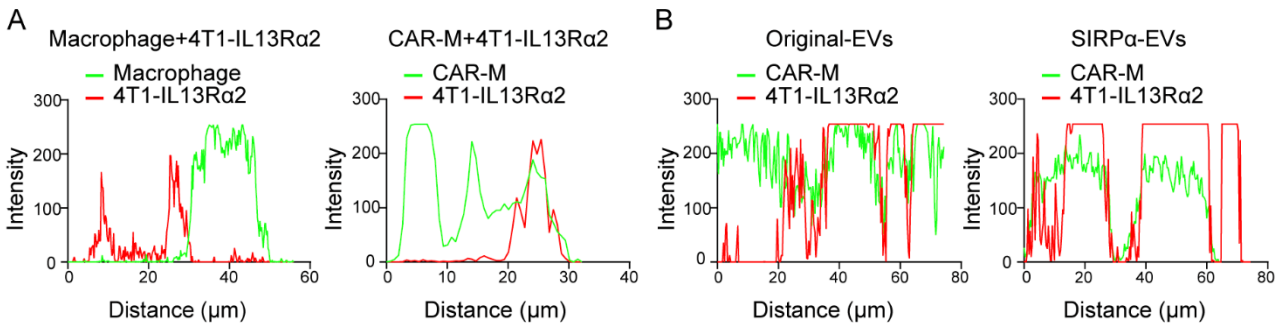

Figure S6. Spectral profiling of phagocytosis under different treatments. (A) Representative fluorescence spectral overlay image showing macrophages (green) and internalized 4T1-IL13Rα2 target cells (red). The purple line indicates the path for spectral profiling (related to Figure 3G). (B) Representative fluorescence spectral overlay image pre-treated with Original-EVs or SIRPα-EVs. Peaks in the green channel overlapping with red peaks indicate co-localization (CAR-M and 4T1-IL13Rα2). The purple line indicates the path for spectral profiling (related to Figure 5H).

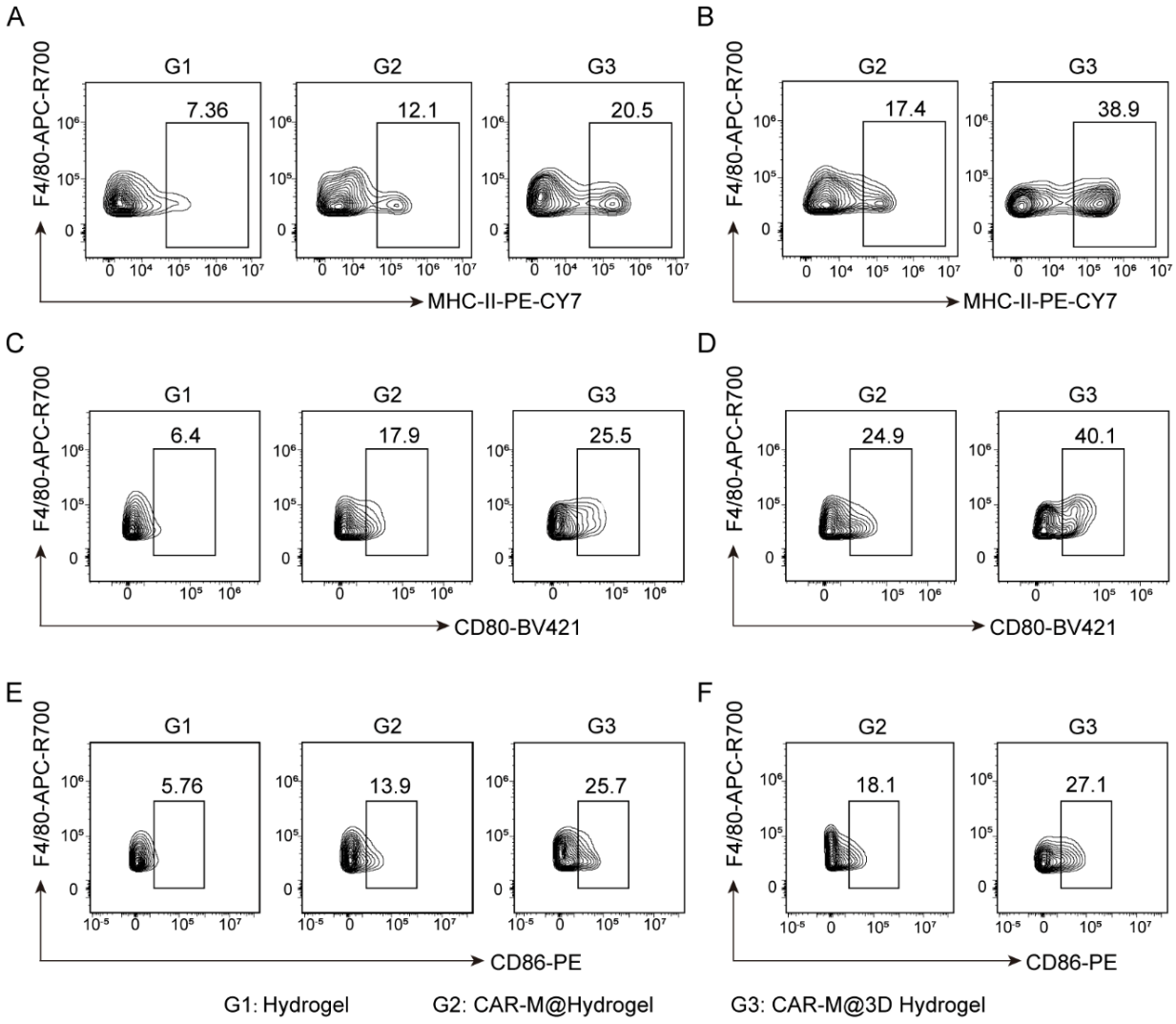

Figure S7. Flow cytometry analysis of macrophage activation markers in tumors. (A-B) Representative flow cytometry plots showing the percentage of MHC-II$^+$ tumor-associated macrophages in CD11b$^+$ F4/80$^+$ cells on day 4 and day 7 post-treatment across different groups (G1, G2, G3). (C-D) Expression of the costimulatory marker CD80$^+$ in CD11b$^+$ F4/80$^+$ cells. (E-F) Expression of the activation marker CD86$^+$ in CD11b$^+$ F4/80$^+$ cells. Data indicate that CAR-M@3D Hydrogel promotes macrophage activation and antigen-presenting function in the tumor microenvironment.

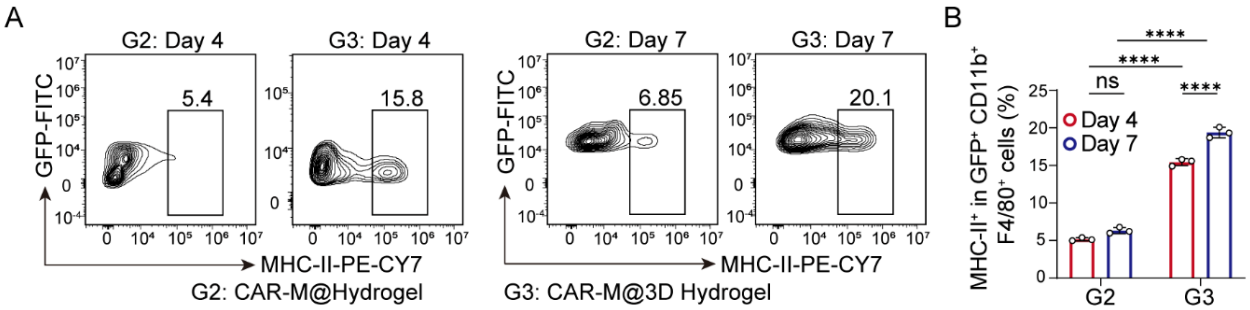

Figure S8. MHC-II expression analysis specifically within the intratumoral CAR-M. (A) The percentage of MHC-II$^+$ cells in GFP$^+$ (CAR-expressing) macrophage subset on days 4 and 7 post-treatment in G2 and G3 groups. (B) The quantitative analysis confirms that CAR-M not only persists but also upregulates antigen presentation machinery within the tumor microenvironment over time. Data are expressed as mean ± s.d. ($n = 3$). Statistical significance was calculated via two-way ANOVA with Tukey's multiple comparisons test. ns, no significance. ****$p < 0.0001$.

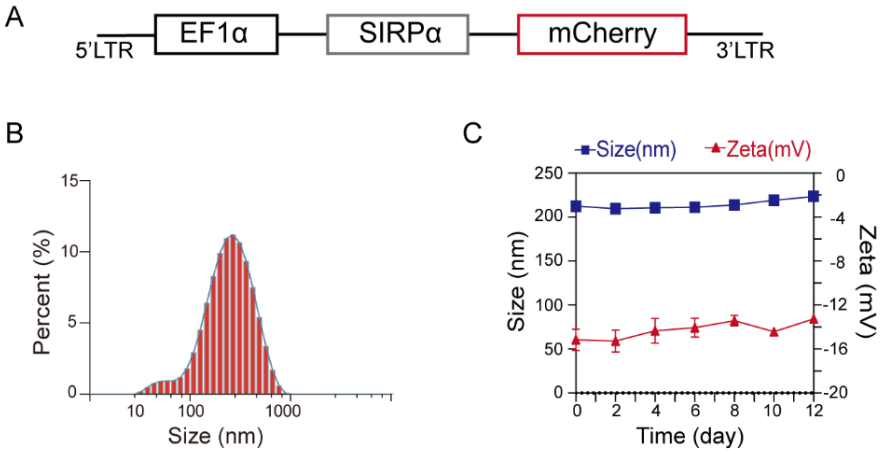

Figure S9. Construction of SIRPα-EVs. (A) Schematic of the lentiviral plasmid used for generating SIRPα-EVs, featuring 5'/3' LTRs, an EF1α promoter driving the expression of a fusion construct containing the SIRPα extracellular domain and mCherry. (B) DLS showing a representative size distribution profile of SIRPα-EVs, with a peak diameter around 150 nm. (C) Stability assessment over time (up to 14 days), plotting the mean hydrodynamic diameter (Size, nm) and zeta potential (Zeta, mV), confirming consistent particle size and surface charge under storage conditions (4 °C).

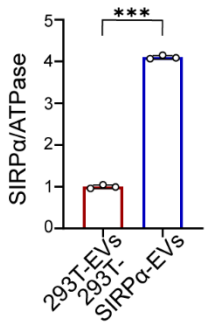

Figure S10. Western blot and quantitative analysis. Quantitative analysis of western blot validating SIRPα expression in transfected 293T (related to Figure 5E). Protein lysates from untransfected 293T-EVs and 293T-SIRPα-EVs were probed with antibodies against SIRPα and ATPase (loading control). Data are presented as mean ± s.d. ($n = 3$). Statistical significance was calculated via unpaired two-tailed t-test. ns, no significance. ***$p < 0.001$.

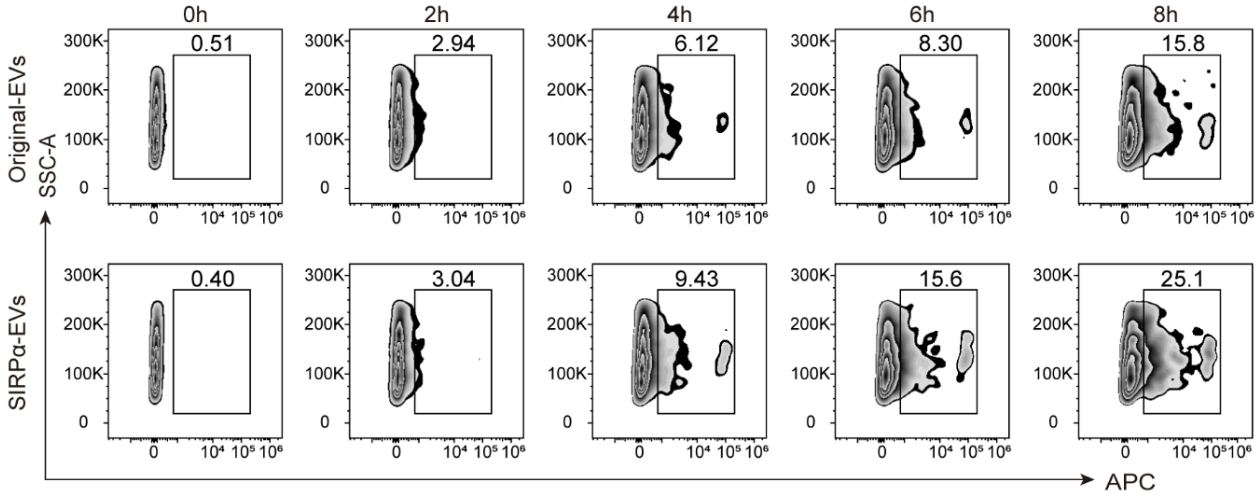

Figure S11. Flow cytometric quantification of phagocytosis. The percentage of APC$^+$ (indicating CAR-M phagocytosis of APC-labeled 4T1-IL13Ra2 cells) over an 8 h co-culture period. Pre-treatment with SIRPα-EVs significantly enhances the phagocytic rate compared to treatment with Original-EVs at all later time points (2 h, 4 h, 6 h, and 8 h).

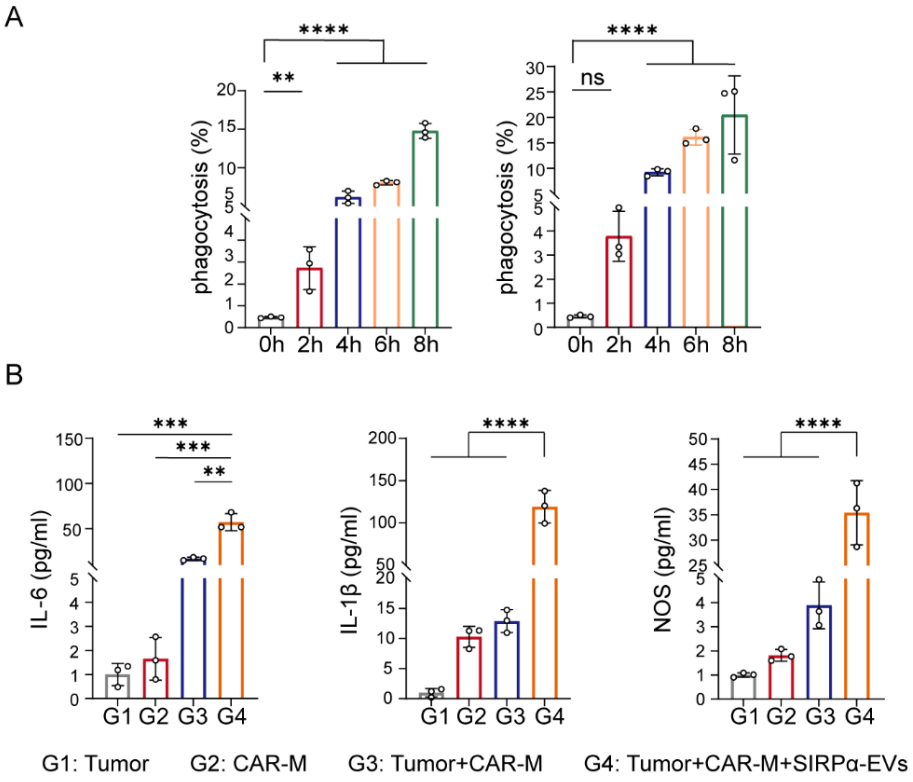

Figure S12. Quantitative analysis of phagocytic activity and cytokine profile. (A) Quantitative analysis of phagocytosis percentage within 8 h. (B) Concentrations of cytokine: IL-6, IL-1β, and nitric oxide synthase (NOS). Data demonstrate that SIRPα-EVs treatment not only significantly boosts phagocytic capacity but also induces a more potent and comprehensive pro-inflammatory response compared to Original-EVs treatment. Data are presented as mean ± s.d. ($n = 3$). Statistical significance was calculated via ordinary one-way ANOVA with a Tukey's test. ns, no significance. ** $p < 0.01$; *** $p < 0.001$; **** $p < 0.0001$.

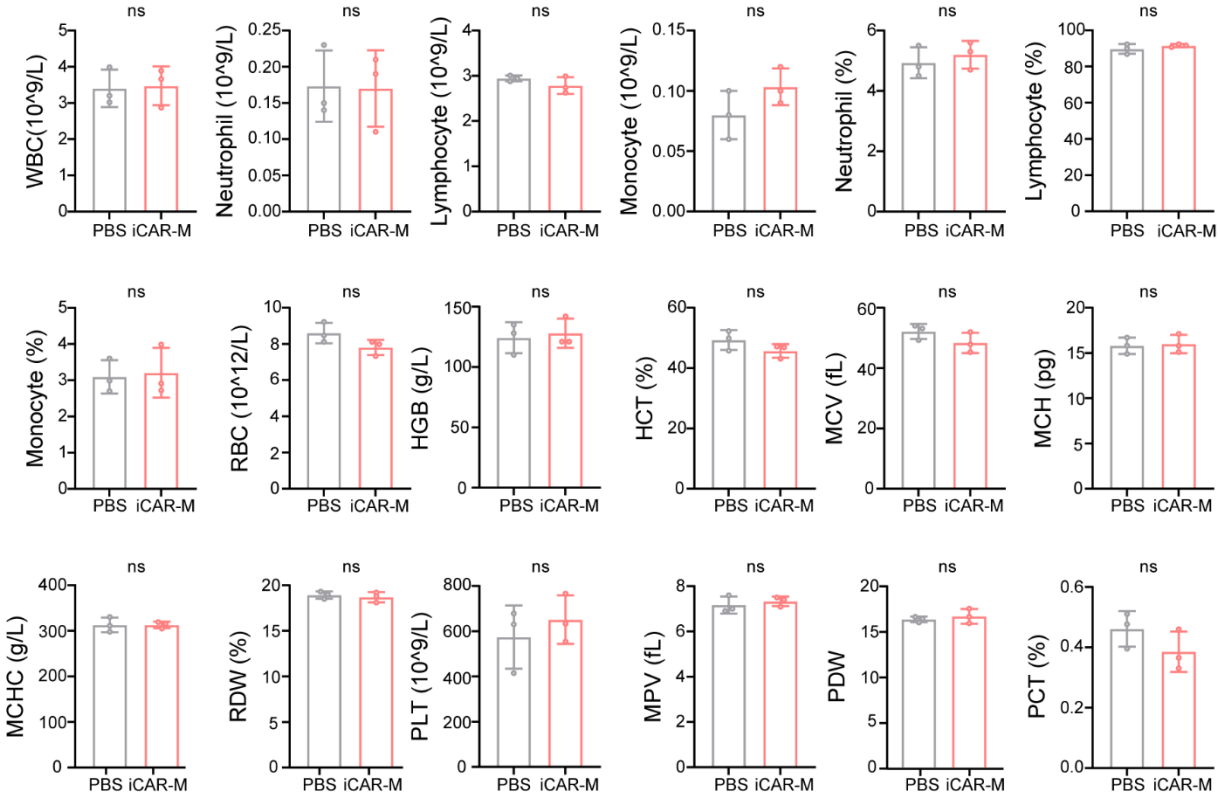

Figure S13. Blood analysis after treatments with PBS and iCAR-M. All data are expressed as mean ± s.d. ($n = 3$). Statistical significance was calculated via unpaired two-tailed t-test. ns, no significance.

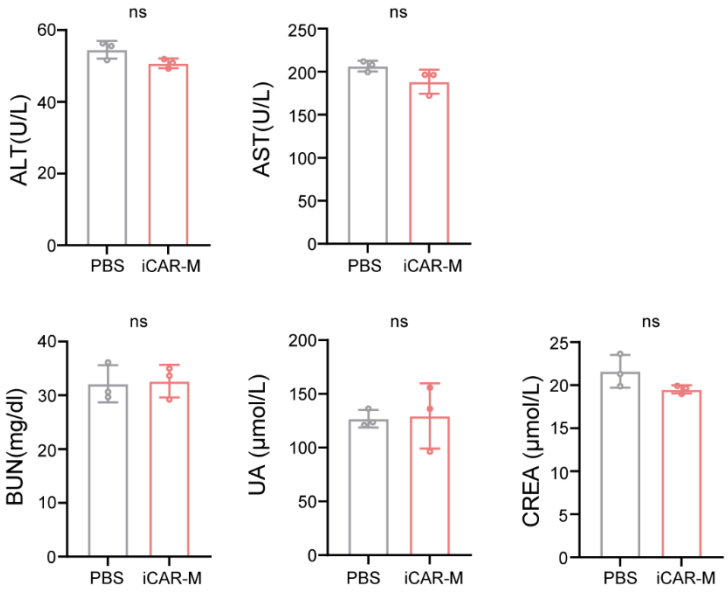

Figure S14. Blood biochemistry analysis after different treatments with PBS and iCAR-M. The relative expression analysis of alanine transaminase (ALT), aspartate aminotransferase (AST), blood urea nitrogen (BUN), uric acid (UA) and creatinine (CREA). All data were expressed as mean ± s.d. ($n = 3$). Statistical significance was calculated via unpaired two-tailed t-test. ns, no significance.

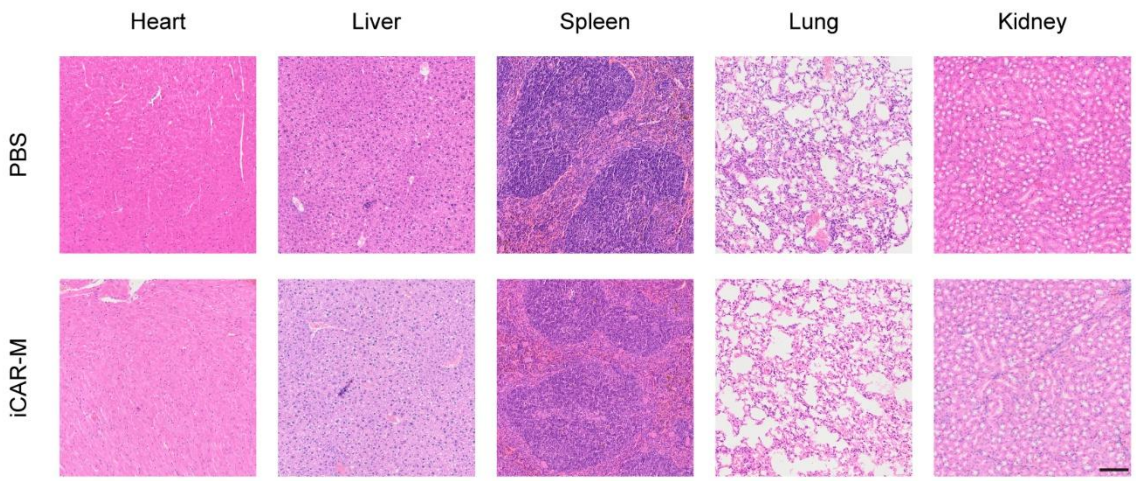

Figure S15. H&E images of tissues after different treatments. The H&E images of heart, liver, spleen, lung, and kidney tissues after different treatments. Scale bar, 100 μm.

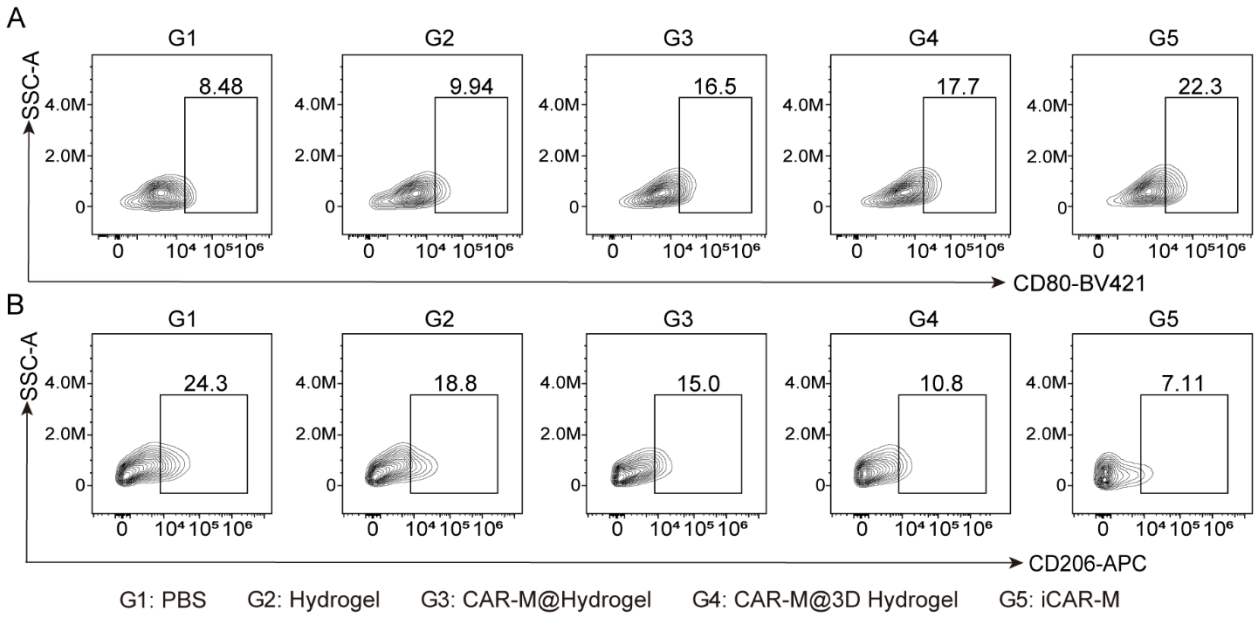

Figure S16. Flow cytometry analysis of activated macrophages in tumor tissues from a post-surgery recurrence model. Representative flow cytometry plots for $CD80^+$ and the $CD206^+$ in $CD11b^+$ $F4/80^+$ cells in tumor tissues in five treatment groups (G1-G5).

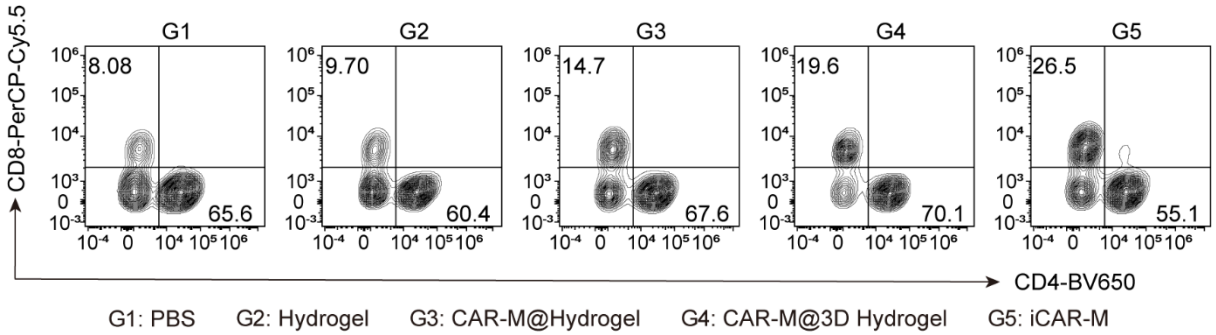

Figure S17. Flow cytometry analysis of T cells in tumor tissues from a post-surgery recurrence model. Flow cytometry analysis of the percentage of $CD8^+$ T cells in $CD3^+$ T cells in tumor tissues in five treatment groups (G1-G5).

Supplemental Table

Table S1. The parameters of 3D printing.

Image	Exp-t	Intst	P-d	Dt1	P-u	Dt2	Scra	Rol
1	20	30	3	0	2.6	20	0	0
2	18	30	3	0	2.6	20	0	0
4	16	30	3	0	2.6	20	0	0

Image: Quantity of images in each stage;

Exp-t: UV exposure time;

Intst: UV intensity;

P-d: Delay time for platform to stay after going down;

Dt1: Delay time for platform to stay after going down;

P-u: Distance for platform to go up;

Dt2: Delay time for platform to stay after going up;

Scra: Frequency of scraper movement;

Rol: Frequency of Roller movement.